Turbulence Intensity Effect on Axial-Flow-Induced Cylinder Vibration

Z. Y. Lu, Y. Zhou and C. W. Wong

Abstract A numerical study is conducted on the effect of inlet turbulent intensity on the axial-flow-induced vibration of an elastic cylinder subjected to axial tubular flow. The cylinder with fix-supported ends is free to vibrate in the lateral direction. While a large eddy simulation is used to calculate the turbulent flow field, the Ansys mechanical + Fluent two-way coupling has been deployed to capture the fluid-structure interaction. The calculation agrees qualitatively with experimental data. Various inlet turbulence intensities, T_u, i.e., 0, 0.3, 5.0 and 10.0%, are examined at two non-dimensional flow velocities, $\overline{U}$, i.e., 3.30 and 7.62. The results show that T_u has a significant effect on the cylinder vibration. At $\overline{U} = 3.30$, the maximum displacement grows with T_u and the vibration is classified as the sub-critical vibration; the instability of cylinder is not induced with increasing T_u. At $\overline{U} = 7.62$, the buckling occurs at $T_u = 0\%$, while the flutter takes place at $T_u = 0.3\%$; both are associated with an asymmetric pressure distribution around the cylinder.

Keywords Axial-flow-induced vibration · Inlet turbulence intensity
Elastic cylinder · Fluid-structure interaction

1 Introduction

Axial-flow-induced vibration of cylindrical structures is frequently seen in engineering. One typical example is that coolant flows through fuel rods in nuclear reactors. The small amplitude vibration produced by flow velocity below the so-called critical velocities for divergence and flutter has been an interest of many

Z. Y. Lu · Y. Zhou (✉) · C. W. Wong
Institute for Turbulence-Noise-Vibration Interactions and Control,
Shenzhen Graduate School, Harbin Institute of Technology, Shenzhen, China
e-mail: yuzhou@hit.edu.cn

Z. Y. Lu
State Key Laboratory of Aerodynamics, China Aerodynamics Research
and Development Center, Mianyang, Sichuan, China

researchers (e.g. [1]). It has been experimentally found that the structural response is sensitive to the flow entrance conditions (e.g. [2]). Furthermore, the incident flow on the clustered fuel rods is always turbulent in practice. However, the information on how the inlet turbulence intensity affects the axial-flow-induced structural vibration is very limited in the literature. This work is to investigate both numerically and experimentally an elastic cylinder subjected to an axial tubular flow with varied incident turbulent intensity T_u. The numerical data is further compared with the experimental data.

2   System Modelling

An elastic cylinder with D in diameter of 0.025 m and $20D$ in length, modelled by Euler-Bernoulli beam, is immersed in a uniform axial tubular flow. Assume an infinitely long cylinder, with no flow separation. The axial flow is confined by a cylindrical wall of the same length as the cylinder and a diameter $12D$, as shown in Fig. 1 where the coordinate system is defined. The cylinder is clamped at both ends so that the end conditions are given by $u|_{z=-10D} = \frac{\partial u}{\partial z}|_{z=-10D} = u|_{z=10D} = \frac{\partial u}{\partial z}|_{z=10D} = 0$. The cylinder may vibrate freely along the x and y directions. The flow boundary conditions at the inlet and outlet are $\nu_{inlet} = (0, 0, \nu_0)$ and $p|_{outlet} = 0$, where ν_0 is the mean axial flow velocity. The non-dimensional velocity $\bar{U}$, time τ, frequency $\bar{f}$ and displacement d_y are defined as follows; $\bar{U} = \nu_0 L \sqrt{\rho A/EI}, \tau = t/L^2 \sqrt{\rho + \rho_c A/EI}$, $\bar{f} = fL^2 \sqrt{(\rho + \rho_c)A/EI}, d_y = u_y(z, t)/D$.
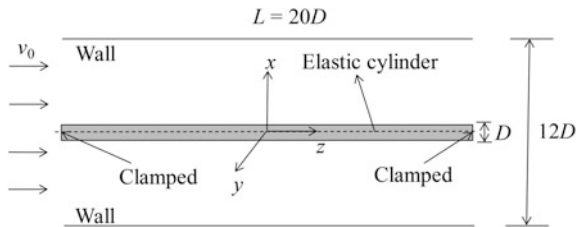
The interactions between the axial flow and the structure are studied by solving iteratively the governing equations of both fluid and structural dynamics. The mass conservation and Navier-Stokes equations along with the structural dynamics equation are given below,

$$\nabla \cdot \vec{\nu} = 0 \tag{1}$$

$$\rho \frac{\partial \vec{\nu}}{\partial t} + \rho(\vec{\nu} - \vec{\dot{\nu}}) \cdot \nabla \vec{\nu} = -\nabla p + \mu \nabla^2 \vec{\nu} \tag{2}$$

$$\mathbf{M}\vec{\ddot{u}} + \mathbf{C}\vec{\dot{u}} + \mathbf{K}\vec{u} = \vec{F}(t) \tag{3}$$

Fig. 1   Schematic model

where t, $\vec{\nu}$, p, ρ, and μ are time, fluid velocity vector, pressure, fluid density and dynamic viscosity of the fluid, respectively; the $\vec{\hat{\nu}}$ refers to the moving mesh velocity vector, and **M**, **C**, **K**, $\ddot{u}$, $\dot{u}$, u and $\vec{F}(t)$ are mass matrix, damping matrix, stiffness matrix, nodal acceleration vector, nodal velocity vector, nodal displacement vector and load vector, respectively. Equations (1)–(3) are iteratively solved by Ansys mechanical + Fluent with two-way coupling [3]. The flow field and the induced forces on the cylinder are solved in each iteration by Ansys Fluent, and then the forces are transferred to Ansys Mechanical to resolving the cylinder displacements. The cylinder displacement is in turn utilized by Fluent to resolving the mesh motion for the next time step. In all cases, there are 6 coupling iterations in each of the 300 subcycles used in the two-way coupling. For turbulent flow, the large eddy simulation (LES) model is applied with Smagorinsky-Lilly for the sub-grid scale (SGS) model, where a Smagorinsky constant C_s is 0.1. The mesh is created by Ansys ICME. To avoid the severe mesh distortion and ensure the mesh quality, the fluid domain is divided into two sub-regions: the inner region where the elements are hexahedrons and the motion of mesh is almost the same as that of the cylinder, and the outer region where the elements are prisms. Grid-refinement studies are performed to ensure that the calculated results are independent of the grid size. The total elements of the mesh in fluid domain are about 688600 for all cases.

3 Results and Discussion

Several values of T_u are examined for $\overline{U}$ = 3.30 and 7.62, which correspond to the Reynolds number based on the hydraulic diameter (= 0.275 m) of 5.88×10^5 and 1.36×10^6, respectively. In all cases, the cylinder is initially at its equilibrium position. In order to validate the computational code, axial-flow-induced cylinder vibration measurements were conducted in a vertical water tunnel. Experiments are conducted for the same model and flow conditions to validate our simulations. The test cylinder is made of silicone rubber, as used by Paidoussis [1] and is fixed vertically with both ends attached to symmetric-airfoil-shaped supporting structures [4]. The experimentally measured root-mean-square (rms) non-dimensional displacement, d_{xrms}, by the Laser Doppler Vibrometer (LDV) at the mid span of the test cylinder agrees well with the calculated results at T_u = 0.3% (Fig. 2).

The d_y at the mid span of cylinder exhibits a considerable dependence on T_u at $\overline{U}$ = 3.30 and $\overline{U}$ = 7.62 (Fig. 3). At $\overline{U}$ = 3.30 and T_u = 0%, d_y is rather small (Fig. 3a), somewhat in an order of 10^{-4}. The maximum d_y grows to about 0.03 and 0.09 at T_u = 5% and 10%, respectively. Based on the magnitude of d_y ($10^{-3} - 10^{-2}D$), the vibrations under various T_u are considered to be subcritical vibration. Apparently, the maximum d_y increases with increasing T_u. It has been captured by our sequential high-speed PIV images from the parallel experimental investigation that vorticity concentrations may separate from the boundary layer around the cylinder as T_u reaches 2.9%, which may have contributed to the enhanced vibration of cylinder. At $\overline{U}$ = 7.62 (Fig. 3b), the cylinder response differently as compared to
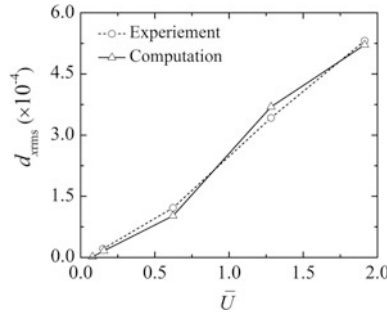
Fig. 2 Comparison of d_{xrms} between computational and experimental measurements ($T_u = 0.3\%$)
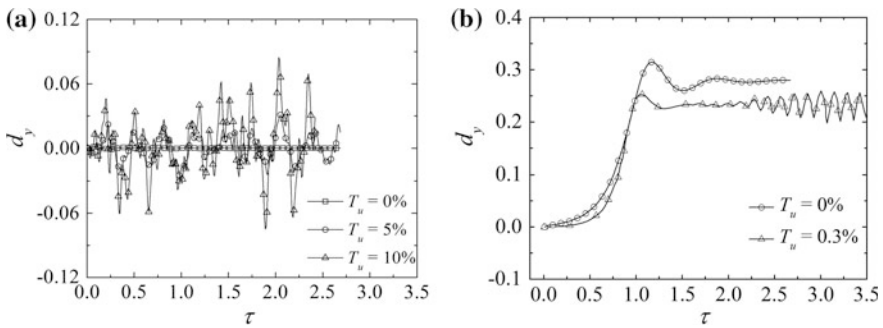

Fig. 3 Time history of d_y at mid-span of cylinder at different T_u. **a** $\overline{U} = 3.30$; **b** $\overline{U} = 7.62$

that at low $\overline{U}$. The d_y increases rapidly at the beginning and eventually reaches a non-zero equilibration vibration state, irrespective of T_u, indicating the occurrence of the buckling instability. The maximum d_y is about 0.3. Given $T_u = 0.3\%$, the buckled cylinder oscillates with an amplitude of about $0.05D$ around its new equilibrium position after $\tau = 2.2$, showing the sign of the flutter instability.

Figure 4 shows the effect of T_u on the d_{xrms} and d_{yrms} along the cylinder span at $\overline{U} = 3.3$ and 7.62. At $T_u = 0\%$, both d_{xrms} and d_{yrms} are very small, about $0.001D$ (Fig. 4a). In addition, at $T_u \geq 5\%$ and $\overline{U} = 3.3$, there exist the second and first modes of subcritical vibration along the x and y directions, respectively. Note that the predominant vibration frequency $\bar{f}$ is a constant (= 3.01), irrespective of T_u, due to the fact that the subcritical vibration has insignificant influence on the flow field. At $\overline{U} = 7.62$, the buckling shape of the cylinder appears to be the first mode of vibration at $T_u = 0\%$, along with the maximum d_{xrms} of about $0.12D$, but changes to the second mode of vibration with the M-shape distribution along the span at $T_u = 0.3\%$ (Fig. 4b). Note that d_{xrms} and d_{yrms} deviate greatly from each other at $\overline{U} = 7.62$, showing the sign of the instabilities of cylinder.

Figure 5 shows instantaneous pressure coefficient (C_p) and vorticity (ω_z^*) contour at the mid span of the buckled cylinder at $\overline{U} = 7.62$ and $T_u = 0\%$. The high and low
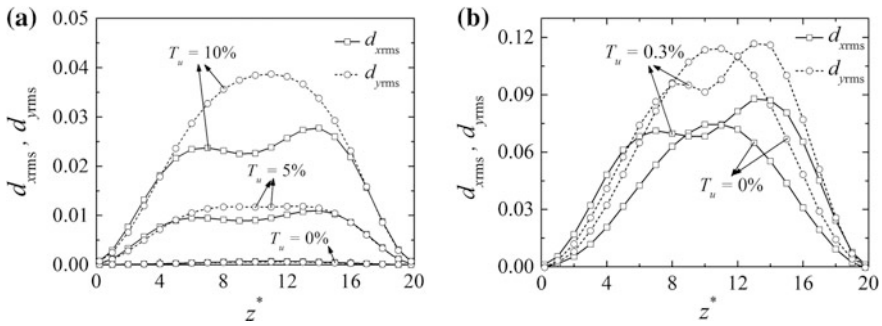
Fig. 4 Root-mean-square non-dimensional displacement. **a** $\overline{U}$ = 3.30; **b** $\overline{U}$ = 7.62
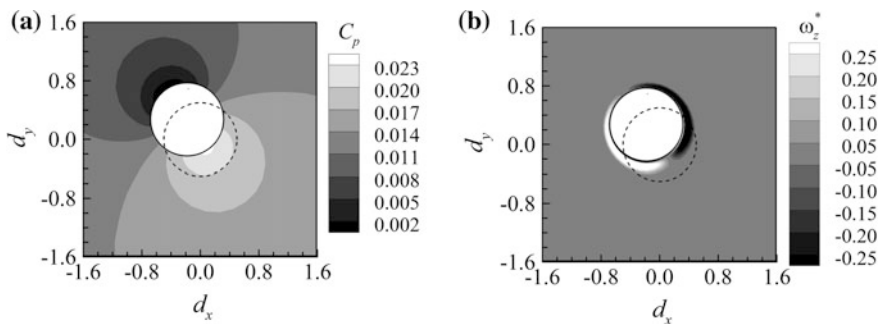

Fig. 5 Instantaneous **a** C_p and **b** vorticity contour at mid span of buckled cylinder. The dotted circle denotes the original position of the cylinder. ($\overline{U}$ = 7.62, T_u = 0%)

pressure regions are found at the inner and outer bend of the buckled cylinder, respectively (Fig. 5a). The maximum C_p may reach about 0.023 at the inner bend of the buckled cylinder. The pressure around the cylinder gives rise to the resultant force on the cylinder which causes cylinder deformation. It is noteworthy that the pressure distribution around the cylinder is not symmetrical along the axis perpendicular to the bending direction. This finding is reasonable. As fluid flows from the outer bend to the inner bend caused by the deformation of cylinder, the shear layers around the cylinder (as inferred from the axial vorticity contours, Fig. 5b) are thickened when approaching to the inner bend, thus resulting in the high-pressure region at the inner bend of the cylinder (Fig. 5a).

4 Conclusions

The effect of the inlet turbulent intensity on the axial-flow-induced vibration of an elastic cylinder is investigated numerically. Calculation has been validated through experiments in a water tunnel. This work leads to following conclusions.

1. At $\overline{U} = 3.3$, the cylinder vibration is subcritical, regardless of the level of T_u. Nevertheless, the maximum d_y of cylinder grows with increasing T_u.

2. At $\overline{U} = 7.62$, the d_y grows rapidly at the beginning and eventually reaches a non-zero equilibration vibration state, irrespective of T_u, indicating the occurrence of the buckling instability. At $T_u = 0.3\%$, the cylinder undergoes buckling with negligible vibration amplitude of about $0.003D$, followed by the flutter instability with a sharp increased vibration amplitude about $0.05D$. The buckling and flutter instabilities take place as a result of the asymmetric pressure distribution along the axis perpendicular to the bending direction.

References

1. Paidoussis MP (2004) Fluid-structure interactions: slender structures and axial flow, vol 2. Academic Press, Netherlands
2. Swinson WF, Battiste RL, Luttrell CR, Yahr GT (1993) Follow-up fuel plate stability experiments and analyses for the advanced neutron source. United States Department of Energy. Oak Ridge National Laboratory, Oak Ridge Tennessee. Technical Report No. ORNL/TM–12629
3. Ansys Workbench 15.0 Document (2015) Ansys Inc
4. Païdoussis MP (1966) Dynamics of flexible slender cylinders in axial flow Part 2. Experiments. J Fluid Mech 26:737–751